C. R. Geoscience 342 (2010) 566–574

Contents lists available at ScienceDirect

Comptes Rendus Geoscience

www.sciencedirect.com

Internal geophysics

Physical properties of fault zones within a granite body: Example of the Soultz-sous-Forêts geothermal site

Propriétés physiques des zones de failles dans un batholite granitique : exemple de l'échangeur géothermique de Soultz-sous-Forêts

Yves Géraud *, Michel Rosener [1], Fabrice Surma [2], Joachim Place [3], Édouard Le Garzic, Marc Diraison

IPGS, UMR 7516, CNRS-UDS, école et observatoire des sciences de la Terre, institut de physique du globe de Strasbourg, université de Strasbourg, 1, rue Blessig, 67084 Strasbourg cedex, France

ARTICLE INFO

Article history:
Received 19 January 2009
Accepted after revision 25 January 2010
Available online 19 March 2010

Written on invitation of the Editorial Board

Keywords:
Granite
Fault zone
Porosity
Permeability
Thermal conductivity

ABSTRACT

In EGS projects, fault zones are considered as the structures controlling deep flow at the reservoir scale. Using a large set of petrophysical properties (porosity, density, permeability, thermal conductivity [TC]) measured on cores collected along the EPS-1 borehole, a model of fault zone is proposed to describe them. A fault zone is a complex structure, showing different parts with different kinds of deformations and/or materials that could explain chemical and physical processes observed during fluid-rock interactions. The different parts composing the fault zone are: (1) the fault core or gauge zone; (2) the damage zone; (3) and the protolith. They are usually heterogeneous and show different physical properties. The damage zone is a potential high permeability channel and could become the main pathway for fluids if secondary minerals seal the fault core. Porosity is the lowest within the protolith, between 0.5 and 1%, but can go up to 15% in the fault zone. Permeability ranges from $10^{-20}\,m^2$ in the fresh granite to, at least, $10^{-15}\,m^2$ in the fault core, and TC ranges from $2.5\,W\,K^{-1}m^{-1}$ to $3.7\,W\,K^{-1}m^{-1}$. Finally, variations in specific surface are set over two orders of magnitude. If the lowest values usually characterize the fresh granite far from fault zones, physical properties could show variations spread over their whole respective ranges within these fault zones.

Mots clés :
Granite
Zone de faille
Porosité
Perméabilité
Conductivité thermique

RÉSUMÉ

Des mesures de propriétés physiques (porosité, densité, perméabilité, conductivité thermique) réalisées sur des échantillons du forage EPS 1 de Soultz-sous-Forêts nous ont permis de proposer un modèle de zone de faille et de distribution des propriétés physiques associées, qui permet d'expliquer la répartition des réactions physicochimiques associées aux interactions eaux-roches. La zone endommagée présente un fort potentiel de transfert qui peut prendre le relais de la zone de gouge, lorsque celle-ci est colmatée par les précipitations secondaires. La porosité est faible en dehors des zones de failles, elle varie entre 0,5 et 1 %, alors

* Corresponding author.
E-mail address: ygeraud@nistra.fr (Y. Géraud).
[1] Geodynamics limited, PO box 2046, Milton QLD 4064, Australia.
[2] CRITT, 19, rue de Saint-Junien, 67305 Schiltigheim, France.
[3] EIFER, Emmy-Noether-Strasse 11, 4th floor, 76131 Karlsruhe, Germany.

1631-0713/$ – see front matter
doi:10.1016/j.crte.2010.02.002

que dans les zones de failles, elle peut atteindre 15 %. La perméabilité varie de 10^{-20} m^2 dans les zones où le granite n'est que peu ou pas altéré à 10^{-15} m^2 dans les zones de failles. La conductivité thermique varie de 2,5 W K^{-1}m^{-1} à 3,7 W K^{-1}m^{-1}, alors que la surface spécifique varie sur deux ordres de grandeur. Si les faibles valeurs de propriétés physiques sont mesurées loin des zones de failles, dans celles-ci, les valeurs des propriétés physiques montrent toutes les gammes de variation.

1. Introduction

The development of high temperature geothermal energy requires a minimum temperature of 200 °C. In Europe, these conditions are realized at limited depth for exceptional high geothermal gradient areas (Iceland or the Larderello geothermal field in Italy), but generally, more or less 5 km depth is required (Gérard et al., 1991). Fluid flow through a geothermal exchanger within a deep reservoir, such as a granitic batholith (a low porosity and permeability material), depends on development of secondary structures like fault and fracture networks, with a good connectivity and permeability. These properties could be estimated by productivity tests and improved by mechanical and/or chemical stimulation processes.

Only few faults or fractures intercepting the boreholes are useable to develop the connected network (Evans et al., 2005), and fluid transfers depend on their aperture, which could control a rapid transfer pathway (Gentier et al., 2000). However, the geometry of a fault zone is more complex than a simple parallel plate model defining a homogeneous space between fault planes: it is composed of a fault core, a damage zone and the protolith (Caine et al., 1996; Sibson and Rowland, 2003). This geometry could control a large set of fluid-rock interactions as well as chemical and physical processes. The aim of this article is the quantification of different physical properties of fault zone materials that was qualitatively described by Genter et al., (2000).

2. EPS-1 borehole and sampling

Different holes were drilled through the Soultz-sous-Forêts granite to generate a circulation at great depth but only one of them (EPS-1) was cored between 1400 and 2300 m in the granite basement. Seventy-nine samples were selected along this core at different depths (see Table 1 for their locations and their petrophysical properties). Previous to the geothermal stimulation, the Hercynian and Alpine phases and especially the Tertiary extensive episode (Villemin and Bergerat, 1987) structured the granite body. This long geological history is associated with tectonic fracturing, hydrothermal fluid circulations, primary minerals dissolution and secondary minerals precipitation that created not only a network of connected open fractures but also porous and extended permeable zones around them (Genter et al., 1990; Genter and Traineau, 1992; Ledésert et al., 1993; Rosener, 2007; Sausse et al., 1998; Sausse, 2002; Surma, 2003).

The petrographic study revealed three types of material: fresh granite, pervasive alteration granite and a fractured-altered granite, (Genter et al., 1990; Genter and Traineau, 1992; Jacquemont, 2002; Ledésert et al., 1993; Rosener, 2007; Sausse et al., 1998; Surma, 2003). Quartz, K-feldspar, plagioclase, biotite and a high density of K-feldspar phenocrysts compose the fresh granite. The first type of alteration is characterised by transformation of primary minerals like biotite, amphibole and plagioclase. Biotite is mainly altered into chlorite and sometimes in celadonite, epidote, hydrogarnet, and carbonates. Plagioclase is mainly altered into corrensite, calcite or illite. The second type of alteration is located in the matrix of the damaged zone and controlled by fluid circulation in and around fractures. The main minerals in the fractures are phyllosilicates (illite, chlorite, tosudite), carbonates and quartz, where the matrix shows mostly illite and carbonates as secondary phases. Schematically, each facies could be characterized by clay phases; the protolith is defined by chlorite formation, the damage zone by the chlorite-illite association, and the fault core by illite. Other clay phases or secondary phases are also present but we choose this simple characteristic for a quick analysis of the samples and their location in the fault model (Table 1, Fig. 1).

3. Techniques

Petrography and chemical data are available through some publications (Genter et al., 1990; Genter and Traineau, 1992; Jacquemont, 2002; Ledésert et al., 1993; Sausse et al., 1998; Surma, 2003). Petrophysical properties are measured on samples selected along the EPS1 core. Four of these are determined: porosity, permeability, thermal conductivity (TC), and specific surface. These parameters control chemical and physical fluid-rock interactions and could be later use to model these processes. All of these measurements are not systematically performed on the same samples, Table 1 summarizes all of obtained data.

Porosity measurement and threshold diameter determination are obtained from a mercury injection test. This technique is based on the Young-Laplace equation for the displacement of a non-wetting fluid in a thin capillary tube, relating the fluid pressure to the throat size. This technique gives access to the total porosity value, but also provides information about the distribution of pore size and pore access diameters. Volume of the samples varies between 3 and 5 cm^3. Due to grain size issues, several samples are used to characterize each facies, in a way to analyse a representative volume.

Permeability measurements are made using a nitrogen gas permeameter working at 40 bars confining pressure. Samples are 18 mm in diameter and 25 mm length. For different constant head pressures (lower than 35 bars) and

Table 1
Sample list: location and physical properties.

Table 1
Liste des échantillons et propriétés physiques.

Sample	Depth	Facies	sp. surface	Density	TC	Porosity	Permeability
K74-2016	1420	AHI			2.31		
K75-2051	1428	AHH					2.95 E − 17
K75 2051	1430.6			2.67	3.17	2.12	3.00 E − 17
K76 2059	1431.9			2.61	3.23		
K76 2061	1432.8			2.59	2.32	3.29	
K79-2128	1455	AHI	4.33 E + 06			2.91	1.75 E − 19
K79-2128	1455	AHI	5.07 E + 06			3.33	9.18 E − 21
K81-2158						0.73	
K81-2191	1471	AHH à AHCH			2.9	5.59	1.93 E − 18
K81-2191	1471	AHH à AHCH			2.96	5.59	1.93 E − 18
K81-2191	1471	AHH à AHCH			2.93	6.92	1.02 E − 18
K81-2191	1471	AHH à AHCH			2.96	6.92	1.02 E − 18
K88-2350	1517	AHH à AHCH			2.81		
K88	1517.5			2.63	3.68	3.1	
K97	1574.3			2.66	3.71	0.34	
K102	1602	Fresh	59100			0.13	5.87 E − 18
K108	1630.5			2.64	2.88	1.03	4.30 E − 17
K108-2758	1631	AHI	5.88 E + 05			1.14	
K108-2758	1631	AHI	1.84 E + 06			1.21	4.09 E − 19
K108-2758	1631	AHI	3.47 E + 06			1.59	4.57 E − 18
K108-2758	1631	AHI				1.97	1.28 E − 18
K109-2782	1637	AHI	1.65 E + 06			0.27	1.82 E − 15
K109-2782	1637	AHI				0.61	5.29 E − 17
K109-2789	1639.1	AHH		2.69	3.59		
K109-2793	1640.5			2.52	2.78		
K109-2794	1641					13.6	
K109-2795	1641.9	AHH	7.41 E + 06			3.93	
K109-2795	1641.9	AHH	1.50 E + 06			1.15	1.58 E − 15
K109-2795	1641.9	AHH	3.52 E + 06			0.81	2.08 E − 17
K109-2795	1641.9			2.6	3.12	5.12	1.30 E − 17
K117	1670.9					0.56	
K117-2900	1679.9	Fresh	1.70 E + 06		2.84	0.82	1.35 E − 17
K117-2900	1679.9	Fresh			2.84	0.22	2.36 E − 17
K117-2900	1679.9	Fresh		2.65	3.45	0.56	
K122	1705.9			2.67	2.92	0.33	
K134-3221	1776.1	Fresh		2.64	2.55	0.56	
K136	1797	Fresh				0.44	
K136	1797	Fresh				0.38	2.14 E − 17
K136	1797	Fresh				0.4	4.63 E − 17
K136a	1797.6			2.68	3.33	0.41	1.00 E − 17
K136b	1797.7					0.41	
K138-3318	1807	AHI	2.51 E + 06			1.82	1.20 E − 18
K138-3318	1807	AHI	2.90 E + 05			0.5	2.90 E − 17
K138-3318	1807	AHI				0.8	1.32 E − 17
K142	1845.3			2.69	3.56	0.71	
K142	1846					0.37	7.79 E − 18
K142	1846					0.36	2.90 E − 20
K150	1905					0.66	
K150-3645	1906	AHI	2.00 E + 06			0.33	8.17 E − 19
K150-3645	1906	AHI				0.4	5.07 E − 18
K150-3645	1906	AHI				0.35	2.44 E − 20
K160-3861	1973			2.65	2.75		
K165	2002	AHI			2.67		
K169-4058	2011			2.69	3.26		
K177-4329	2053	AHCS	1.49 E + 06			1.75	1.63 E − 20
K178-4329-4	2070					9.1	
K178	2071					10.58	
K179-4349	2076.4					0.18	
K191	2142	Sain			2.59		
K193	2152	AHI	4.26 E + 06		3	3.92	7.37 E − 18
K193	2152	AHI	5.74 E + 06		3	5.07	1.70 E − 18
K193-4693	2154.9						
K195-4755	2168			2.67	3.7	2.3	
K195-4755b				2.66	3.85		
K195-4772	2160.5				2.53		
K195-4774	2161		7.07 E + 06		2.48	8.62	1.44 E − 18
K195-4774	2161		1.00 E + 07			9.87	7.59 E − 19

Table 1 (*Continued*)

Sample	Depth	Facies	sp. surface	Density	TC	Porosity	Permeability
K195-4774	2161		8.49 E + 06			7.83	5.38 E – 19
K195-4777	2162	AHCS			3.49		
K195-4782	2163	AHI			2.77		
K195-4779-1	2174					2.53	
K195-4779-2	2174.4					2.53	
K195-4779-3	2174.4					2.53	
K197	2179.7			2.69	3.12		
K206-4984	2214.5					0.29	
K207-5009-1	2220.5						
K207-5009-2	2220.6			2.67	3.4		
K207-5019	2222					0.56	
K207-5028	2224.5	Fresh			2.69		

Depth (m); Facies AHI: Illite-Hematite association, AHH: Hematite, AHCH: Chlorite-Hematite association; Fresh; Sp. surface (m2.g-1); Density g.cm-3; TC (W.K-1.m-1); Porosity (%); Permeability (m2)

once the steady-state condition is reached, gas flow rates and pressures from the both sides of the samples (the head and foot pressures) are recorded. These values must be corrected for the Klinkenberg effect to obtain the real permeability value (Scheideffer, 1974; Debschutz et al., 1989; Klinkenberg, 1941). For several samples, these experimental conditions are not sufficient to measure flow and they are defined as impermeable, with permeability lower than 10^{-20} m^2. It is also important to notice that these experimental conditions are much different from the deep in situ conditions.

To determine the TC, we use the optical scanning technique developed by Popov et al. (1999). With a measurement taken every 1 mm, TC normal to the analysed surface is determined as an arithmetic average of local conductivity along an entire scanning line. The

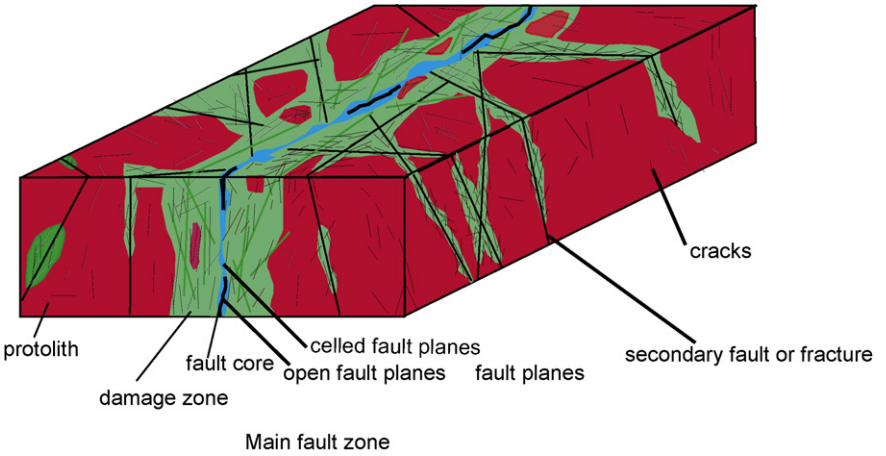

Fig. 1. The block diagram proposes a conceptual model for fault zone built from the Caine's model (Caine et al., 1996) using the data acquired from the EPS1's holes core of the Soultz–sous-Forêts granite. Three kinds of structures are represented: the main fault zone, composed itself from the centre to the edge by the fault planes, the fault core, the damage zone and the protolith; the associated fracture network which presents the same structure than the fault zone but the extension of the different parts is more reduced; and then the cracks network. Three materials are used to build this model. First is the protolith in red, (Group 1 of the Fig. 5), it is characterized by low porosity value, voids composed by cracks, and a sharp increase of the permeability for an increasing porosity is measured. It composes the external part of the fault zone, with a very low porosity value, but some lenses are recognized in the damage zone or near the fault core; within these, the porosity is increased and the permeability is very high. The second material (in green) forms the damage zone with factures and cracks but the alteration of the matrix is very important, the porosity is increased and the permeability behaviour is complex and depends on the development of secondary minerals that control the tortuosity factor. The third material is localized in the fault core, with a high increase of the porosity by fracturing and mineral dissolution, but a part of this volume is filled by secondary phases, and could be completely closed. The fault core material (in blue) is a high porosity material, but the permeability is decreased by the secondary mineral precipitation. The fault itself, i.e. between the both fault planes, could be open or closed by mineral precipitation or breccias accumulation.

Fig. 1. Ce bloc représente un modèle de zone de faille à partir du modèle de Caine et al., (1996) selon les données acquises sur les échantillons d'EPS-1. Trois grands types de structures sont représentés : la faille principale elle-même comprenant du centre vers la périphérie, les plans de faille, le noyau de la faille, la zone endommagée et le protolithe ; les structures secondaires qui comprennent les mêmes éléments que la faille principale, mais avec des extensions plus limitées ; le réseau de fissures. Les différents faciès qui composent le batholithe granitique sont résumés à trois matériaux dans ce modèle. Le premier est le protolithe en rouge (groupe 1 de la Fig. 5), le matériau a une faible porosité, les vides sont de type fissure, la perméabilité augmente fortement pour une faible variation de porosité. Ce matériau compose la partie externe des zones de failles, avec une très faible porosité, mais des lentilles sont reconnues dans la zone endommagée ou dans le noyau de la faille ; dans ces lentilles, la porosité augmente et la perméabilité est forte. Le second type de matériau forme la zone endommagée (en vert) avec un fort développement de la fracturation et de la fissuration ; l'altération de la matrice est importante, la porosité est fortement augmentée et la perméabilité présente une évolution complexe dont l'augmentation est contrôlée par le développement de la fissuration et la diminution par la précipitation de minéraux secondaires. Le matériel du noyau de la faille (en bleu) présente une forte porosité, mais une perméabilité plus faible du fait de la précipitation de minéraux secondaires. La faille elle-même, c'est-à-dire l'espace entre les deux plans de failles, peut être ouverte ou colmatée par des produits secondaires.

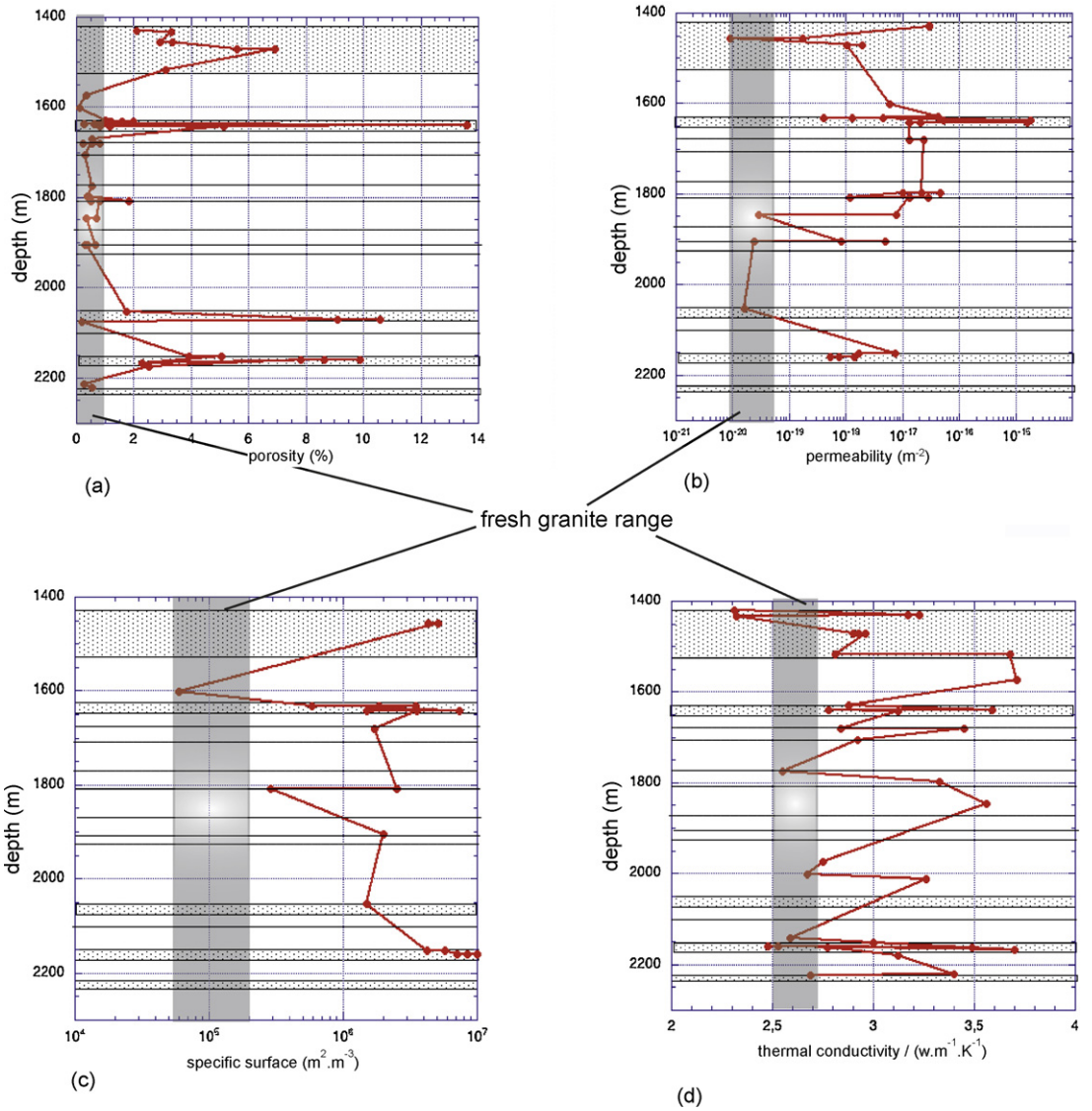

Fig. 2. Physical properties: a: porosity; b: permeability; c: specific surface; d: thermal conductivity. All of these properties present a large variability in the different fracture zones. **a**: porosity. The matrix porosity value of the fresh granite is around 0.5%. The highest values are measured in the fracture zones and the surface alteration zones (grey zones), the main and some minor fracture zones show higher porosities, up to 15%; **b**: permeability. Fracture zones present a large variation, with lower value than the fresh granite ($10^{-20} - 10^{-19}$ m^2). In the major fracture zones, permeability variation is over three orders of magnitude and can reach 10^{-15} m^2; **c**: specific surface value ranges over two orders of magnitude and the highest values are measured in the damage zone; **d**: thermal conductivity varies between 2.3 and 3.7 W.m^{-1}.°C^{-1}. Fresh granite value ranges from 2.5 to 2.7 W.m^{-1}.°C^{-1}. Fracturing induces lowest values, highest values are induced by secondary mineral phases precipitation (quartz and calcite).

Fig. 2. Propriétés physiques : **a** : porosité ; b : perméabilité ; c : surface spécifique ; d : conductivité thermique. Toutes ces propriétés montrent une grande variabilité dans les zones de fractures : a : porosité. La porosité de la matrice du granite sain est d'environ 0,5 %. Les valeurs les plus élevées sont mesurées dans les zones de fractures et dans la zone d'altération ; l'augmentation de la porosité est plus importante dans les larges zones de fracture, les zones moins épaisses voient leur porosité également augmentée ; **b** : perméabilité. Les zones de fractures montrent une grande variabilité avec des valeurs faibles comparables à celles qui sont mesurées pour les granites sains ($10^{-20} - 10^{-19}$ m^2). Dans les zones de fractures principales, les valeurs des perméabilités peuvent atteindre 10^{-15} m^2 ; **c** : les valeurs de surface spécifique varient sur plus de deux ordres de grandeur ; les valeurs les plus élevées sont mesurées dans les zones endommagées de la zone de faille ; **d** : les valeurs de conductivités thermiques varient entre 2,3 et 3,7 W.m^{-1}.°C^{-1}. Les valeurs mesurées pour le granite sain sont comprises entre 2,5 et 2,7 W.m^{-1}.°C^{-1}. Les valeurs plus faibles correspondent à des échantillons fissurés, les valeurs plus élevées sont dues à des phases secondaires (quartz et calcite) qui ont précipité dans les réseaux de fracture.

relative measurement error is not more than 2% (Popov et al., 1999). Measurements are performed on samples that are 10 to 20 cm long; some of them were re-sampled afterwards for permeability measurements. Compared to other techniques, the optical scanning allows both average and pinpoint evaluations.

The BET method (Brunnauer et al., 1938) is used for specific surface area (SSA) measurements. At low tem-

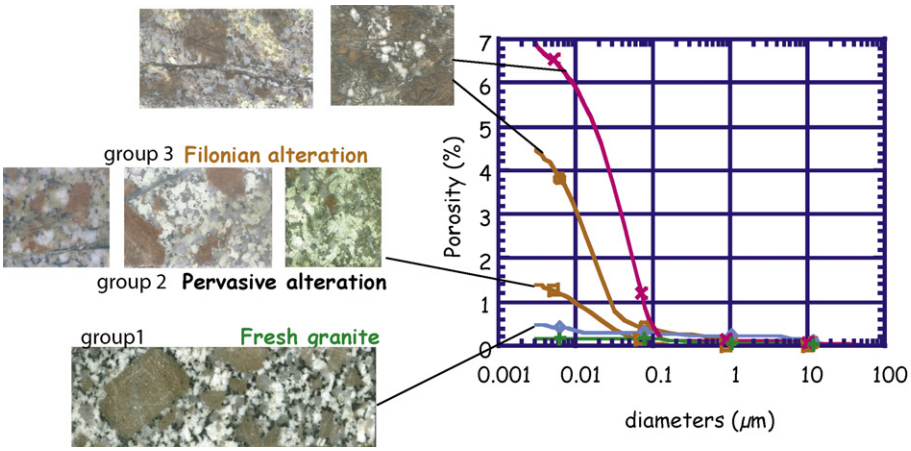

Fig. 3. Porosity volume distribution versus threshold values. Increase of the porosity volume is associated to an increase of the threshold values. This behaviour is the result of the cracking and of the alteration of primary mineral phases.

Fig. 3. Répartition du volume poreux en fonction des seuils d'accès. L'augmentation de la porosité est associée à l'augmentation de la taille des seuils d'accès. Cette évolution est la conséquence de la fracturation et de l'altération des phases primaires.

perature and low pressure, gas is adsorbed on the porosity network surface (Gregg and Sing, 1982). By measuring the quantity of gas adsorbed at different pressures, it is possible to estimate the specific surface of the sample (in $m^2\,g^{-1}$ or $m^2\,m^{-3}$). Nitrogen is used for our measurement.

Using SEM observations, void shapes and voids relationships with mineral components are determined to define the link between the different physical properties. Observations are performed on ships of rocks under a GEOL scanning electronic microscope.

4. Results

All of the results are summarized on the Fig. 2. Two main types of information come from the mercury injection technique, the porosity value and the distribution of the pore volume versus the threshold value. Porosity ranges from 0.5% to up to 15% and its variation is not depending on the depth of sampling. It is controlled by the location of the sample within the fault zone. Samples from the protholith have porosity as low as 0.5%. In the damage zone, porosity can increase up to 15%, and lower values can also be measured near the fault core. Porosity in the fault core varies over two orders of magnitude.

With regard to the EPS-1 well, four high porosity zones are recognized, three of them linked to fracture zones at 1620, 2070 and 2120 m depth (Fig. 2). The fourth is located at the upper part of the batholith on the Hercynian unconformity, where alteration of the granite's top and post Permian/Triassic fluid flow induced high porosity at the granite-sedimentary cover contact. Zones with lower porosity are also localized along secondary fracture zones, as at 1800 m depth. Low fracture density characterises these secondary fracture zones.

The porosity increase could be linked to an increase of the threshold values (Fig. 3). Different porosity spectra could be recognized, from relatively flat spectra for the low porosity material to a porosity network controlled by a particular threshold value, where the porosity increase is associated with the threshold increase. These porosity variations are measured on small volume samples (3 or $5\,cm^3$) and describe matrix porosity and microcracks porosity development.

Permeability varies over five orders of magnitude from $10^{-20}\,m^2$ to $10^{-15}\,m^2$ (Fig. 2). Several high permeability zones are recognized with permeability values higher than $5.10^{-17}\,m^2$. In several cases, these zones could be related to high porosity zones like at 1620 or 2120 m depth, but in other cases, these high permeability zones are not linked to high porosity like at 1800 or 1900 m depth. Conversely, high porosity zones are not related to high permeability volume. This could be due to lack of permeability samples or to low cracking of the matrix around different fault zones. In the alteration zone of the upper part of the batholith, a large variation of the permeability is measured over three orders of magnitude. The permeability–porosity relationship is complex (Fig. 4) and depends on the pore structure, voids geometry and location (Fig. 5). Three types of behaviour could be distinguished depending on the porosity shape (Rosener and Géraud, 2007). For the cracks network (group 1), a sharp increase of the permeability is measured for a low porosity increase. The second group (group 2) is composed of samples where alteration and secondary phase precipitation modify the pore structure. Under these conditions the permeability decreases with porosity. Samples of the group 3 are intensively cataclased and illite and chlorite precipitate in the enlarged cracks and pores by mechanical and chemical processes. For low porosity samples, the permeability increases with porosity, and for porosity above 4% the permeability decreases. These particular relationships (decrease) between the porosity and the permeability are clearly the illustration of the tortuosity effect controlled by the infilling development in the cracks networks and the alteration of the primary phases. Especially for the group 3, the threshold value being constant for all the samples of the group, porosity parameters (volume and threshold) increase and

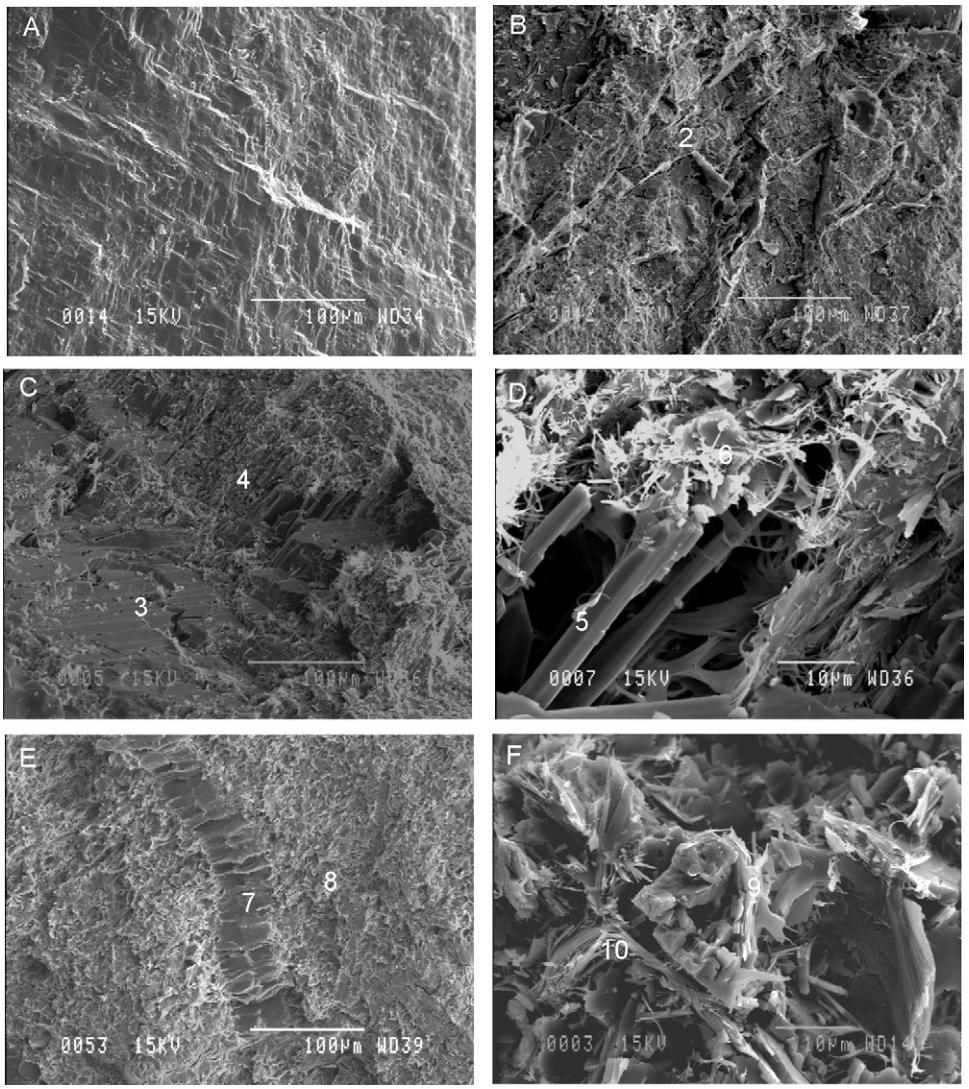

Fig. 4. Some SEM views. **A**. (K-134 at 1779 m deep), unaltered feldspar without alteration glyphs, twining in the K-feldspar are only visible (1). **B**. (K-109 at 1639 m deep), cracks network in a feldspar, 3 directions could be recognized, and some of them are filled by clay minerals (2). **C**. (K-81 at 1471 m deep), intensively altered feldspar with corrosion glyphs (3), dissolution of K-feldspar and clay precipitation (4). **D**. Detail of C, only some columns of the feldspar are preserved (5) and illite mineral is largely developed (6). **E**. (K-194 at 2155 m deep), calcite fills the cracks (7) in a highly altered matrix (8) that could explained the high thermal conductivity value measured for samples with high porosity. **F**. (K-194 at 2155 m deep), clays formation in the altered matrix with kaolinite (9) and illite (10).

Fig. 4. Images en microscopie électronique. **A**. (K-134 profondeur 1779 m), Feldspath sans figure d'altération visible et macle dans un cristal de feldspath - K, peu altéré (1). **B**. (K-109, profondeur 1639 m), réseau de fissures dans un feldspath, trois directions de fissures peuvent être identifiées, certaines de ces fissures sont remplies par des argiles (2). **C**. (K-81, profondeur 1471 m), cristal de feldspath très fortement altéré avec des figures de corrosion (3), d'altération et des cristallisations d'argiles (4). **D**. Détail de C, seules des colonnes subsistent dans le cristal de feldspath (5) et les cristallisations d'illite sont fortement développées (6). **E**. (K-194, profondeur 2155 m), des cristaux de calcite remplissent des fissures (7) dans une matrice très altérée (8) ; ce phénomène peut expliquer les fortes valeurs de conductivité thermique mesurées pour certains échantillons à forte porosité. **F**. (K-194, profondeur 2155 m). Formation d'argiles dans une matrice altérée, à kaolinite (9) et illite (10).

the permeability decreases. They illustrate the influence of the tortuosity increase.

The SSA is not measured for all the samples, but a similar tendency like the ones described for permeability and porosity is observed, i.e. a large variation is measured for samples coming from the fractured zone. However, a simple relationship with permeability or porosity could not be found. The highest values are measured on samples coming from two fracture zones at 1660 and 2100 m depth. The altered zone in the upper part of the batholith gives also samples with high SSA value. These high values are directly linked to the clay content of the sample, whereas the lowest SSA is measured for the unaltered and little fractured samples (Rosener and Géraud, 2007).

TC varies between 2.3 $W K^{-1} m^{-1}$ and 3.7 $W K^{-1} m^{-1}$. TC for the fresh granite lies between 2.5 $W K^{-1} m^{-1}$ and

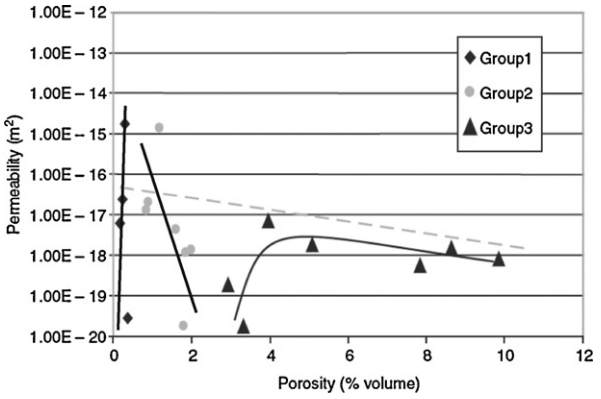

Fig. 5. Porosity-permeability relationship. Three relationships could be described. The group 1 concerns the fresh granite and the cracked samples, for a low increase of the porosity value, the permeability increases sharply. The group 2 shows the same range of permeability than the previous one but permeability increase seems associated to a light porosity increase. The group 3 is composed by samples coming from the damage zone: for an increasing porosity value, the permeability first increases and then decreases. The first phase of permeability behaviour is associated to the crack network development; the second one is controlled by the secondary phase precipitation and the increase of the tortuosity.

Fig. 5. Relation porosité-perméabilité. Trois relations peuvent être identifiées. Le premier groupe correspond au granite sain et aux échantillons fracturés : pour une faible augmentation de la porosité, la perméabilité augmente fortement. Le groupe 2 montre la même gamme de variation de perméabilité que le groupe précédent, mais l'augmentation de perméabilité est liée à une décroissance de la porosité. Le troisième groupe comprend les échantillons venant de la zone endommagée : pour une porosité croissante la perméabilité évolue en deux temps ; le premier est une augmentation due au développement de la fissuration, la seconde phase correspond à une diminution de la perméabilité qui traduit une augmentation de la tortuosité due à la précipitation de phases secondaires.

$2.7\,W\,K^{-1}m^{-1}$, in accordance with the literature (Cermak and Rybach, 1982; Pribnow and Sass, 1995; Rummel, 1991; Surma and Géraud, 2003). As for the other properties, TC presents large variations within the fractured zones. Decrease of the TC value is the result of the porosity development by fracturing or by mineral alteration. This process is particularly obvious across the altered zone at the top of the batholith, where the lowest values are measured. On the other hand, a large part of the tested samples shows an increase of the TC value with alteration. This evolution is clearly associated to secondary phase precipitations, especially quartz with a TC value of $7.69\,W\,K^{-1}m^{-1}$ and calcite with a mean TC value $5\,W\,K^{-1}m^{-1}$. This TC increase could mask the effect of the porosity development.

5. Discussion: a fault zone model

From these data, physical properties of a theoretical fault zone may be proposed. A first qualitative geometry of the fault zones in the Soultz's batholith was proposed by Genter et al.(1995). Here after, our model is the synthesis of data coming from different Phd theses (Jacquemont, 2002; Rosener, 2007; Surma, 2003), their mineralogical and chemical point of view is developed in Fritz et al. (this volume). Using the model proposed by Caine et al., 1996 and Sibson and Rowland, 2003, a more refined synthesis of the fault zone could be drawn and analysed samples could be localised on this model. Essentially, a set of altered conjugate structures with lower offset is associated to the principal fault.

The central part of the main structure is described as the fault core: a highly strained material, with large ranges of porosity and permeability depending on the degree of cementation. It can also include locally open sections that could support high fluid flow after being reconnected during the stimulation. The second part is the damage zone, where previously fractured material is subject to alteration and secondary precipitations. Generally, the increase of porosity induced by fracturing and mineral dissolution is higher than the decrease of porosity associated with secondary mineral precipitation. However, due to their nature (mostly clays) secondary precipitations generate high tortuosity, and so tend to decrease the permeability of the rock (group 3 material). In these damage zones, there are also some preserved rock volumes of which some small porosity increase related to sharp permeability increase is unclear but probably induced by a crack network development (group 1). These volumes (fault core and damage zone) are generally not connected to the protolith or other preserved blocks. The last part of the system is the protholith that remains largely unaffected by the fault.

The global geometry and physical properties profile across the fault zone could be described as follows: within the damage zone, from the protolith to the fault core, permeability increases due to fracturing and primary phase alteration. Then, toward the fault plane, it could be reduced by secondary mineral precipitation (Lockner et al., 2000). Between the two surfaces of the fault plane, occasional free space could represent a high fluid flow conduit with high permeability; where in other sections, this volume could be filled more or less completely, possibly showing a lower permeability than the surrounding material. In the last case, the damage zone would then be the section showing the highest permeability. Finally, connections between the fault core and the damage zone are made possible via several secondary structures that could, at their own scale, present a similar layout as the main fault zone.

This geometry explains the high frequency variation of the different physical properties measured in the fault zones or the fractured zones and also the large variations of transport properties recognized along the borehole. It is also in accordance with the conceptual model proposed by Caine et al., 1996, where the size of the fault core and the damage zone could vary as well as their transport properties.

6. Conclusion

Petrophysical characterizations of different samples coming from the EPS1 core are used to build a fault zone model of the deep geothermal reservoir. The different elements of this fault zone are the open space between the fault planes, the fault core, the damage zone and the protolith. The characteristics of each part point out the role of the damage zone as a high porosity and permeability

zone. In particular, it could be a pathway for the fluid if the fault core is filled by impermeable secondary phases. Across the fault zone, even if structure sizes are variable, petrophysical properties of the damage zone seem to be more consistent than in the fault core, where fluid-rock interactions are more intense and induce bigger variations.

Acknowledgements

F. Surma and M. Rosener were funded by "Région Alsace" and ADEME for their PhD; ADEME and Eifer supported J. Place for his PhD. This research program was supported by a European Community grant "STREP". "Région Alsace" contributed to the founding of the Thermal Conductimeter. Many thanks to all of them for their constant support. Many thanks to the both anonymous reviewers for their constructive remarks.

References

Brunnauer, S., Emmett, P.H., Teller, E., 1938. Adsorption of gases in multimolecular layers. J. Amer. Chem. Soc. 60, 309–319.

Caine, J.S., Evans, J.P., Forster, C.B., 1996. Fault zone architecture and permeability structure. Geology 24, 1025–1028.

Cermak, V., Rybach, L., 1982. Thermal conductivity and specific heat of minerals and rocks, In: Landolt and Börnstein V/1: Physical properties., G. Angenheister, Editor. Springer. pp. 305-344.

Debschutz, W., Kruckel, U., Schopper, J.R., 1989. Effect of geostatic stress and pore pressure on the klinkenberg permeability factor and other fluid parameters. In: Proceedings of the symposium "Rock at great depth", Pau.

Evans, K.F., Genter, A., Sausse, J., 2005. Permeability creation and damage due to massive fluid injections into granite at 3.5 km at Soultz: 1. Borehole observations. J. Geophys. Res. 110 .

Genter, A., Cautru, J.P., Montaggioni, P., Traineau, H., 1990. Geological interpretation of well logging data from the granitic section of the Soultz-sous-Forêts well GPK1. The Log Analyst 31, 35.

Genter, A., Traineau, H., 1992. Borehole EPS1, Alsace, France. Preliminary geological results from granite core analysis for hot dry rock research. Scientific Drilling 205–214.

Genter, A., Traineau, H., Dezayes, C., Elsass, P., Ledésert, B., Meunier, A., Villemin, T., 1995. Fracture analysis and reservoir characterization of the granitic basement in the HDR Soultz project. Geothermal Science and Technology 4, 189–214.

Genter, A., Traineau, H., Ledésert, B., Bourgine, B. and Gentier, S., 2000. Over 10 years of geological investigations within the HDR Soultz project, France. In: World Geothermal Congress 2000, Kyushu - Tohoku, Japan.

Gentier, S., Hopkirk, D., Riss, J., 2000. Role of fracture geometry in the evolution of flow path under stress, In: Dynamics of fluids in fractured rock, geophys. Monogr. Ser., B. Faybishenko, P. Witherspoon, and S.M. Benson, Eds. AGU: Washington D.C. pp. 169–184.

Gérard, A., Kappelmeyer, O., Rummel, F., Ferrandes, R., Schloemer, W., Benderitter, Y., 1991. European HDR project at Soultz-sous-Forêts. Geothermal Science and Technology 3, 7–9.

Gregg, S.J., Sing, K.S.W., 1982. Adsorption surface area and porosity, 2nd Ed. Academic press, London, , 303 p.

Jacquemont, B., 2002. Étude des interactions eaux-roches dans le granite de Soultz-sous-Forêts. Quantifications et modélisations des transferts de matière pour les fluides, PhD thesis, université Louis Pasteur: Strasbourg, 181 p.

Klinkenberg, L.J., 1941. Permeability of porous media to liquid and gases. American petroleum institut, drilling and production practice 2, 200–213.

Ledésert, B., Dubois, J., Velde, B., Meunier, A., Genter, A., Badri, A., 1993. Geometrical and fractal analysis of a three-dimensional hydrothermal vein network in a fractured granite. J. Volcanol. Geotherm. Res. 56, 267–280.

Lockner, D.A., Naka, H., Tanaka, H., Ito, H., Ikeda, R., 2000. Permeability and strength of core samples from the Nojima fault of the 1995 Kobe earthquake, In: Proceedings of the International Workshop on the Nojima Fault Core and Borehole Analysis: U.S. Geological Survey.

Popov, Y.A., Pribnow, D.F.C., Sass, J.H., Williams, C.F., Burkhardt, H., 1999. Characterization of rock thermal conductivity by high-resolution optical scanning. Geothermics 28, 253–276.

Pribnow, D., Sass, J.H., 1995. Determination of thermal conductivity for deep boreholes. J. Geophys. Res. 100, 9981–9994.

Rosener, M., 2007. Étude pétrophysique et modélisation des transferts thermiques entre roche et fluide dans le contexte de l'échangeur geothermique de Soultz-sous-Forêts, PhD thesis, université Louis Pasteur, 204 p.

Rosener, M., Géraud, Y., 2007. Using physical properties to understand the porosity network geometry evolution on gradually altered granites in damage zones., In: Rock Physics and Geomechanics in the Study of Reservoirs and Repositories, Special Publication of Geological Society of London, London, pp. 175–184.

Rummel, F., 1991. Physical properties of the rock in the granitic section of the borehole GPK1, Soultz-sous-Forêts. Geothermal Science & Technology 3, 199–216.

Sausse, J., 2002. Hydromechanical properties and alteration of natural fracture surfaces in the Soultz granite (Bas-Rhin, france). Tectonophysics 348, 169–185.

Sausse, J., Genter, A., Leroy, J.L., Lespinasse, M., 1998. Description et quantification des altérations filonniennes : paléoécoulements fluides dans le granite de Soultz-sous-Forêts (Bas Rhin, France). Bull. Soc. geol. France 169, 655–664.

Scheidegger, A.E., 1974. The physics of flow through porous media. 3rd Ed. University of Toronto Press, 353 p.

Sibson, R.H., Rowland, J.V., 2003. Stress, fluid pressure and structural permeability in seismogenic crust, North island, New Zealand. Geophys. J. Inter. 154, 584–594.

Surma, F., 2003. Relation entre les caractéristiques minéralogiques, chimiques et physiques des matériaux granitiques du site géothermique de Soultz-sous-Forêts., PhD thesis, université Louis Pasteur, Strasbourg, 321 p.

Surma, F., Géraud, Y., 2003. Porosity and thermal conductivity of the Soultz-sous-Forêts granite. Pure and Applied Geophysics 160, 1125–1136.

Villemin, T., Bergerat, F., 1987. L'évolution structurale du fossé rhénan au cours du Cénozoique : un bilan de la déformation et des effets thermiques de l'extension., Bull. Soc. geol. France 3, 245–256.